# BEYOND CLASSICAL DIFFUSION: BALLISTIC GRAPH NEURAL NETWORK

**Anonymous authors**
Paper under double-blind review

## ABSTRACT

This paper presents the ballistic graph neural network. Ballistic graph neural network tackles the weight distribution from a transportation perspective and has many different properties comparing to the traditional graph neural network pipeline. The ballistic graph neural network does not require to calculate any eigenvalue. The filters propagate exponentially faster($\sigma^2 \sim T^2$) comparing to traditional graph neural network($\sigma^2 \sim T$). We use a perturbed coin operator to perturb and optimize the diffusion rate. Our results show that by selecting the diffusion speed, the network can reach a similar accuracy with fewer parameters. We also show the perturbed filters act as better representations comparing to pure ballistic ones. We provide a new perspective of training graph neural network, by adjusting the diffusion rate, the neural network's performance can be improved.

## 1 INTRODUCTION

How to collect the nodes' correlation on graphs fast and precisely? Inspired by convolutional neural networks(CNNs), graph convolutional networks(GCNs) can be applied to many graph-based structures like images, chemical molecules and learning systems. Similar to neural networks, GCNs rely on random walk diffusion based feature engineering to extract and exploit the useful features of the input data. Akin to neural networks(NNs), promising improvements have been achieved by defining the diffusion-based filters and using them in a multi-layer NN.

Recent works show random walk based methods can represent graph-structured data on the spatial vertex domain. For example, Li et al. (2017) use bidirectional random walks on the graph to capture the spatial dependency and Perozzi et al. (2014) present a scalable learning algorithm for latent representations of vertices in a network using random walks. Except for the spatial domain, many researchers focus on approximating filters using spectral graph theory method, for example,Bruna et al. (2013) construct a convolutional architecture based on the spectrum of the graph Laplacian; Defferrard et al. (2016) use high order polynomials of Laplacian matrix to learn the graphs in a NN structure model.

Though the spectral domain method involves operation like solving the eigenvectors $|\Psi\rangle_{i1}^{n-1}$ of the graph Laplacian $L = I_n - D^{-1/2}WD^{-1/2}$, where $n$ represents the dimension of the data, e.g. the total number of vertices on a two dimensional image-based graph proposed in Defferrard et al. (2016), $I_n$,$D$,$W$ is the identity, degree and weight matrix respectively. From the diffusion perspective, the spatial and spectral methods are attributed to the same diffusive category. For example, for a $k$ step random walk on the one-dimensional infinite line with no biased walk, the final probability distribution of the random walk will converge to applying $L^k$ on the initial state. The distance from the start point of a simple random walk will converge to $C\sqrt{k}$, where $C$, $k$ is the constant and the number of total steps respectively. [1].

[1] there are many discussions about random walk asymptotic behaviour, for example, please see: `https://www.mit.edu/~kardar/teaching/projects/chemotaxis(AndreaSchmidt)/more_random.htm`, `http://mathworld.wolfram.com/RandomWalk2-Dimensional.html` and `http://www.math.caltech.edu/~2016-17/2term/ma003/Notes/Lecture16.pdf`

## 2 RELATED WORK

The authors fail to find related papers that go beyond the classical diffusion frame or tackle the problem from a transportation perspective. By controlling the speed of diffusion, our model changes the weight distribution on different nodes by using ballistic diffusion. This method circumvents increasing the complexity of existed diffusion model or complex matrix calculation(such as inversion or calculate the eigenvalue of a matrix). The related work we find is:

**Graph Attention Networks** Graph Attention Networks enables (implicitly) specifying different weights to different nodes in a neighbourhood. The authors use $e_{ij} = a(W\vec{h_i}, W\vec{h_j})$ to indicate the correlation between vertex $i$ and $j$. By selecting the $N_i$ nodes in the neighbourhood, they assign different importance to nodes of the same neighbourhood. However, adding attention to the graph, though changes the weight distribution, makes the pipeline more cumbersome and lack of physical insight.

## 3 THE SPEED PROBLEM

The random walk/Laplacian matrix is employed for collecting the correlated information over a graph. Here we consider a two-dimensional condition, taking the start point as (0,0) and the correlated point is ($i$,$j$), the distance is denoted as $d_{ij}$. As discussed, the distance walker travelled is $C\sqrt{k}$, in this case, though a $\lceil d_{ij} \rceil$ step walker can reach ($i$,$j$), the probability distribution on the correlated point is relatively low since the walker's average distance is $C\sqrt{k}$. In order to fully capture the correlation between the two vertices(in other words, increase the weight between (0,0) and ($i$,$j$)), two main methods are used:

1. take steps $\lceil d_{ij} \rceil^2$ steps, in Defferrard et al. (2016), in analogy to a 5×5 filter, the authors use Laplacian polynomial order up to 25 to achieve a similar accuracy, the number of steps is far larger than the filter's size in CNNs.
2. Pooling: the distance of two vertices are shortened after pooling operation. $\lceil d_{ij} \rceil$ will reduced to $\lceil d_{ij}/2 \rceil$/ after a 2 ×2 pooling. e.g. Henaff et al. (2015) and Bruna et al. (2013) use max pooling, Defferrard et al. (2016) use efficient pooling and Tran et al. (2018) use sort pooling.

Figure 1 shows the relation between the distance and number of steps for the random walk/Laplacian matrix. As the steps increases, the walker diffuse with the distance $\sim \sqrt{k}$, where $k$ is the number of steps, resulting in the inefficiency in collecting information. Suggested by Hammond et al. (2011), the filter on most common graph convolutional network is:

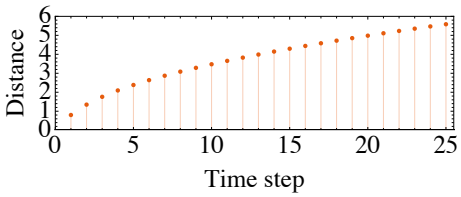


Figure 1: Classical diffusion

$$g_\theta(L)x = g_\theta(U\Lambda U^T)x = Ug_\theta(\Lambda)U^T x \qquad (1)$$

$g_\theta(\Lambda) = \sum_{k=0}^{K-1} \theta_k \Lambda^k$ and $\theta \in R^K$ is a vector of polynomial coefficients. The number of steps corresponds to the polynomial order of the Laplacian. However, as the number of steps grows, the distance walker travelled changes slower and slower, resulting in low efficiency and duplicated filters.

In the next section, we will introduce the ballistic walk method that instead of walking at classical diffusion speed, the walker is able to reach an average distance $\sim Ck$ in $k$ steps walking. Being different from the classical diffusive transportation, this method enables us to collect correlation faster.

## 4 BALLISTIC WALK ON GRAPH

In the following, we will focus on the regular graphs to demonstrate the ballistic graph neural network, where image, video and speech data are represented.

### 4.1 INTRODUCTION TO BALLISTIC WALK

The ballistic walk algorithm consists of two parts, a walker in the position space $\mathcal{H}_{spatial}$ and a coin in the coin space $\mathcal{H}_c$. Thus the walker is described using states in Hibert space $\mathcal{H}_{spatial} \otimes \mathcal{H}_c$. Let the walker initially be at the state $|\Psi\rangle_0 = |i,j\rangle_p \otimes s_0$, where $s_0$ is normally a symmetric state in $\mathcal{H}_c$. In analogy to the classical random walk, the next state of the walker can be expressed by $|\Psi\rangle_{t+1} = \widehat{\mathcal{U}} |\Psi\rangle_t$, where $\widehat{U}$ consists two operations, a flip operation $\widehat{O}_{coin}$ in the coin space and shift operation $\widehat{S}$ in the spatial space.

In this paper, we consider the ballistic walk on a regular two-dimensional graph. The coin space $\mathcal{H}_c$ consists of four states: $|\downarrow\rangle$, $|\uparrow\rangle$, $|\leftarrow\rangle$, $|\rightarrow\rangle$, represents move up, down, left and right for the next step. The spatial space $\mathcal{H}_{spatial}$ consisits $N$ states representing the walker's position, where $N$ is the number of nodes. The notation $|n\rangle$ denotes an orthonormal basis for $\mathcal{H}_{spatial}$ and $\langle n|$ is the Hermitian conjugate of the state. For a finite-dimensional vector space, the inner product $\langle n'|n\rangle$ is $\delta_{nn'}$ and the outer product $|n'\rangle \langle n|$ equals to a matrix in $R^{N\times N}$. The probability stay on the node $|i,j\rangle$ is $\sum_{s=\downarrow,\uparrow,\leftarrow,\rightarrow} \left\| \langle \Psi \, |i,j\rangle \otimes |s\rangle \right\|^2$. Pseudo-code of our method is given in Algorithm 1.

**Algorithm 1:** Ballistic walk on 2D regular graph

**Result:** The walker's state after K steps start from $(i,j)$

$p_0 = |i,j\rangle$ // The start point

$s_0 = a\,|\downarrow\rangle + b\,|\uparrow\rangle + c\,|\leftarrow\rangle + d\,|\rightarrow\rangle$ // $a,b,c,d \in \mathbb{C}; \|a\|^2 + \|b\|^2 + \|c\|^2 + \|d\|^2 = 1$

$\widehat{S} = \sum_{i,j} \mid i-1,j\rangle\langle i,j \mid \otimes |\uparrow\rangle\langle\uparrow| + \sum_{i,j} \mid i+1,j\rangle\langle i,j \mid \otimes |\downarrow\rangle\langle\downarrow| + \sum_{i,j} \mid i,j+1\rangle\langle i,j \mid \otimes |\rightarrow\rangle\langle\rightarrow| + \sum_{i,j} \mid i,j-1\rangle\langle i,j \mid \otimes |\leftarrow\rangle\langle\leftarrow|$

$\widehat{O}_{coin} = \mathcal{H} \otimes \mathcal{H}$ //$\mathcal{H}$ is usually the Hardmard matrix

$|\Psi_0\rangle = p_0 \otimes s_0$

$|\Psi_1\rangle = \widehat{S}(p_0 \otimes s_0)$

**for** $i = 2;\ i < K;\ i = i+1$ **do**

  $|\Psi_i\rangle = \widehat{S}(\widehat{O}_{coin}\,|\Psi_{i-1}\rangle)$

**end**

### 4.2 EXPERIMENTS

The experiment is performed on the MNIST dataset, The Hadmard matrix $\mathcal{H}$ is $\frac{1}{\sqrt{2}}\begin{bmatrix}1 & 1\\ 1 & -1\end{bmatrix}$ and the initial state is $\Psi_0 = 1j/2\,|\uparrow\rangle + 1/2\,|\downarrow\rangle - 1j/2\,|\leftarrow\rangle - 1/2\,|\rightarrow\rangle$. Figure 2 and 3 show the difference in diffusion between the random walk based diffusion and the ballistic diffusion on a $28 \times 28$ grid starting from the center. Comparing to the classical random walk, the ballistic walker shows cohesive behaviour and transports faster. The comparison between the speed is shown in Figure 4.

The diffusive classical walker's distances at $time = 15$ and $time = 20$ center around the same range. The ballistic walkers' differences are more significant, which means collecting different information. Comparing to classical random walk, the ballistic walker has a speed of $\sim k$. This linear transportation behaviour enables the filters collect correlation on graph more efficiently.

As shown in Figure 4, the distance for a diffusive walk at $time = 25$ is around taking an 8-step ballistic walk. Defferrard et al. (2016) considers 25 steps diffusive filters to approximate a $5 \times 5$ kernel with 10 feature maps(10 hidden units). For comparison, we take an 8-step-ballistic kernel with the same number of feature maps. The feature maps are then fully connected to 10/32 units and then connected to 10 units for classification. The notations are denoted as Ball10 and Ball32. Table 1 summarizes the capabilities of our model compared to other recent modeling approaches.

**Baselines** We compare our approaches with the following baselines:

- **DeepWalk**: Perozzi et al. (2014) uses local information obtained from truncated random walks. For iterating over all the vertices of the graph, the authors generate a random walk $|W_{v_i} = t|$ for every node, and then use it to update representations.

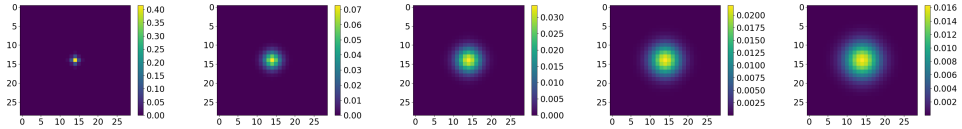

(a) Step: 1 (b) Step: 5 (c) Step: 10 (d) Step: 15 (e) Step: 20

Figure 2: The classical diffusion at different steps

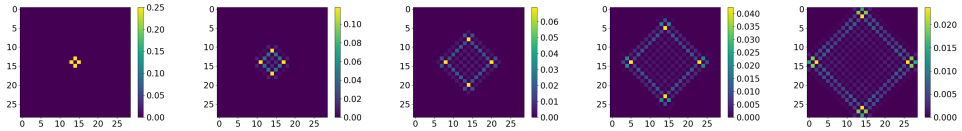

(a) Step: 1 (b) Step: 5 (c) Step: 10 (d) Step: 15 (e) Step: 20

Figure 3: The ballistic diffusion at different steps

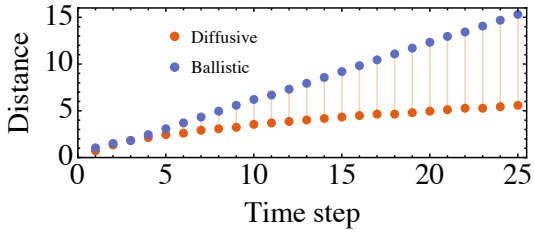


Figure 4: The diffusion behaviour of ballistic and diffusive walk.

- **Graph Attention Networks (GAT)**: Veličković et al. (2017) assigns different weights to different nodes in a neighbourhood. The graph attentional layer changes the weight distribution on the neighbourhood nodes.
- **Manifold Regularization (ManiReg)**: Belkin et al. (2006) brings together ideas from the theory of regularization in reproducing kernel Hilbert spaces, manifold learning and spectral methods. In the paper, their propose data-dependent geometric regularization method based on graph Laplacian.
- **Graph Convolutional Network (GCN)**: Kipf & Welling (2016) conducts the following layer-wise propagation in hidden layers using random walk based method($X^{(k+1)} = \sigma(D^{-1/2}AD^{-1/2}X^{(k)}W^{(k)})$). The final perceptron layer for classication is defines as: $Z = softmax(D^{-1/2}AD^{-1/2}X^{(k)}W^{(k)})$.
- **Graph Learning-Convolutional Networks(GLCN)**: Jiang et al. (2019) contains one graph learning layer, several graph convolution layers and one final perceptron layer. The layer-wise propagation rule is: $X^{(k+1)} = \sigma(D_s^{-1/2}D^{-1/2}X^{(k)}W^{(k)})$.

## 5 Revisit the speed problem

In the last section, we introduce the ballistic walk, which transports faster than the diffusive classical walk. By selecting the ballistic filters up to $K = 8$, we reach $97\%$ and use 1/3 parameters comparing to spline method using classical diffusive filters. This suggests ballistic filters are able to collect correlation more efficiently comparing to random walk based Laplacian filters.

Figure 6 shows the transportation behaviour of different kinds of filters. There exists two phases: 'trapped to diffusive' phase and 'diffusive to ballistic' phase. The laplacian-based filters can be seen as the up-bound filters of the trapped to diffusive phase(the orange points) and obey the $\sqrt{steps}$ law. As the steps grow, the filters are inefficient. As shown in the Figure 6, the filters are repeatedly sampling the region with distance$< 10$ as the steps grow up to 70 steps, this means the filtered information can be very similar, leading to invalid feature layers. The ballistic filters lie at the up-bound of the 'diffusive to ballistic' phase(the blue points), the linear propagation ensures gathering the long

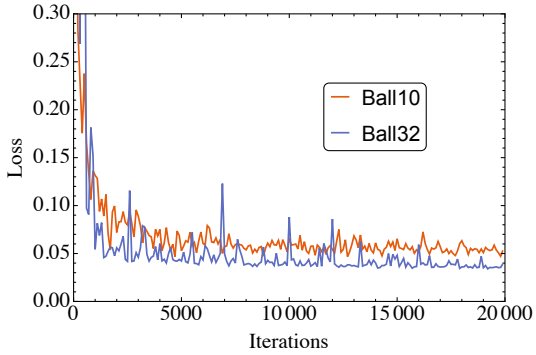


Figure 5: Results of one layer Ballistic graph network with 10 and 32 hidden units on MNIST dataset. The feature layers include 8 ballistic filters.

| Structure | Ball10 | Ball32 | GC10(Non-Param) | GC10(Spline) | GC10(Cheb) |
|---|---|---|---|---|---|
| Accuracy | **97.21**(K=8) | **97.38**(K=8) | 95.75(K=25) | 97.26(K=25) | 97.48(K=25) |
| Structure | ManiReg | DeepWalk | GCN | GAT | GLCN |
| Accuracy | 94.62 | 95.34 | 91.01 | 92.81 | 95.46 |

Table 1: Results on MNIST dataset using Ballistic filters with K = 8 compared with traditional diffusion-based graph convolutional network with K = 25 in Defferrard et al. (2016)

.

correlation information in a relatively small number of steps. However, linear transportation also brings drawbacks:

- Sparse sampling at the mid-distance region: as shown in Figure 6 (figure in the figure), for a 35-steps walker, the points from $distance = 6$ to $distance = 13$ enables the ballistic filters can better interpret the long correlation. However, the distance intervals between the ballistic filters are relatively sparse, and this can result in the missing some correlation.
- Beyond the boundary: the linear ballistic transportation makes the walker go beyond the boundary (for our case the distance is 14). With the same number of the steps, the ballistic walker travels to the boundary line(shown in Figure 7).

Is there a way to generate filters that can collect the correlation within $distance < 14$ area while circumventing cumbersome classical diffusion? In other words, we are interested in generating filters with a transportation speed between ballistic and classical diffusion. By controlling the speed of the filters, we circumvent going beyond the boundary and make all our filters localized between the regions with restricted distance(denoted as the diffusive to ballistic phase in Figure 6).

## 6 De-coherence

In the ballistic diffusion, we use Hardmard transformation on the coin space, The Hardmard operator (SU(2)) helps spilt the state in the coin space and finally leads to linear ballistic transportation. However, as mentioned in the last section, we are interested in generating filters lines between ballistic and classical phase so that we can circumvent the boundary and slow-transportation problem. In this section, we introduce the de-coherence scheme to perturb ballistic transportation by adding a noise term to the Hardmard operation at every step. This noisy perturbation results in the de-coherence of ballistic filters and thus slows down the transportation.

### 6.1 The introduction to decoherence

We want our filters have a diffusion distance in a reasonable region($a < Distance < b$). However, the ballistic filters' distances increase with steps. The filters are not capable to dense sampling some specific regions. By selecting different randomness and steps, we can generate filters localized in a

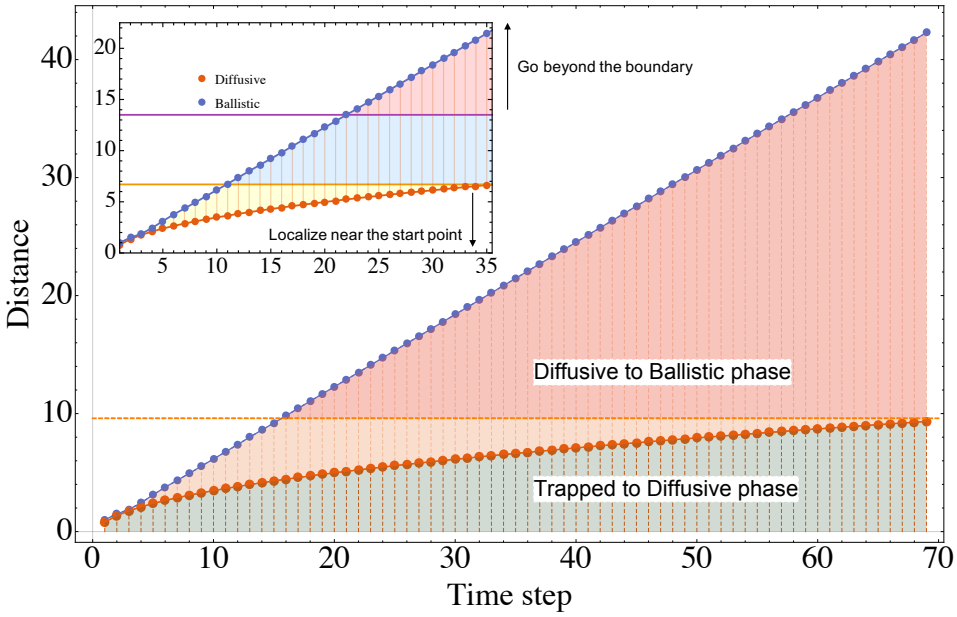


Figure 6: Comparison between diffusive and ballistic transportation. Cassical diffusive walker transports slower and localizes near the start point, and ballistic walker moves beyond the boundary as steps grow. We are interested in learning the information with in the $28 \times 28$ gird.

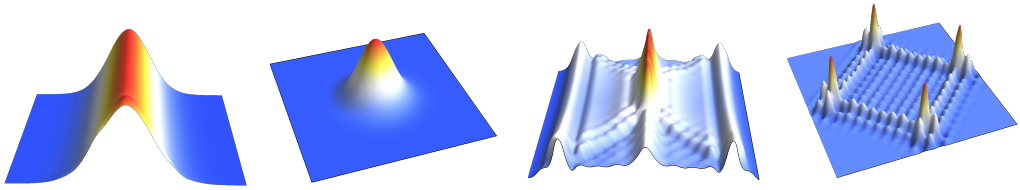

(a) (b) (c) (d)

Figure 7: Comparison between ballistic and classical transportation. (a) Classical diffusion started from a line; (b) Classical diffusion started from a point; (c) Ballistic diffusion started from a line; (d) Ballistic diffusion started from a point. The ballistic filters have the exceeding boundary problem.

bounded area. The noisy Hardmard can be written as

$$H_r(\beta) = \begin{bmatrix} 1 & e^{i\beta} \\ e^{-i\beta} & -1 \end{bmatrix} \tag{2}$$

Table 3 shows the accuracy with different perturbated filters($\alpha = 0, 0.05, 0.10, 0.15, 0.20$). $\beta = 2 \times R \times \pi\alpha$ denotes the randomness in the coin space, $R$ is a random number between 0 and 1. The corresponding transportation speed is shown in table 2. As the $\alpha$ increases to 0.20, the speed drops to 0.323. $\alpha$ is a controller of the diffusion speed, as $\alpha$ becomes larger, the ballistic tranportation will finally evolve to the classical diffusive couterpart.

| Randomness | $\alpha = 0$ | $\alpha = 0.01$ | $\alpha = 0.05$ | $\alpha = 0.1$ |
|---|---|---|---|---|
| Speed | 0.612 | 0.608 | 0.586 | 0.516 |
| Randomness | $\alpha = 0.15$ | $\alpha = 0.20$ | $\alpha = 0.25$ | $\alpha = 0.30$ |
| Speed | 0.414 | 0.323 | 0.268 | 0.240 |

Table 2: Diffusion rate with different randomness

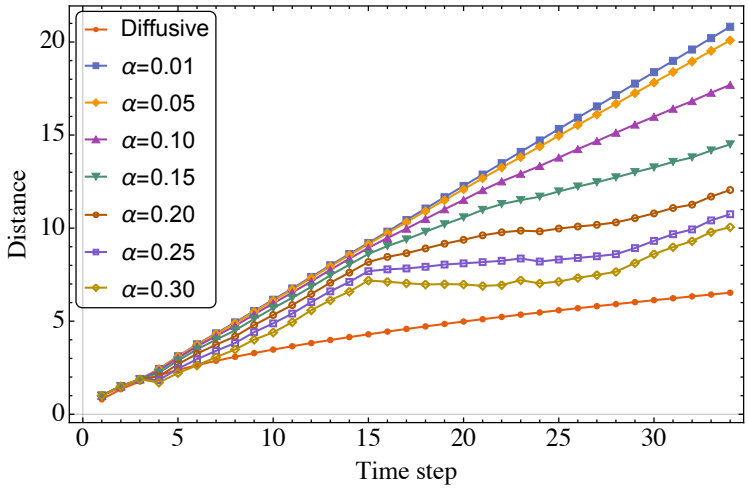


Figure 8: Comparison between diffusive and ballistic transportation with different random Hardmard operator.

### 6.2 SUMMAY OF THE SPEED WITH RANDOMNESS

After taking randomized operations, the accuracy can be improved. In other words, by using filters from the perturbed ballistic walk, we are now able to dense sample the 'meaningful regions' and avoid the shallow sampling and slow transportation problem by selecting the step and the randomness of the ballistic walker. The 'meaningful regions' are denoted as blue and yellow in Figure 6 (figure in the figure). In our model, we fix the first eight filters as the pure ballistic filters without perturbation. We

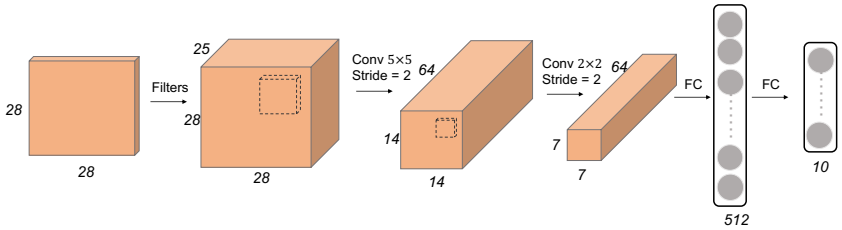


Figure 9: The model architecture with 25 filters as feature maps

then select different filters from perturbed filters. The model architecture is shown in Figure 9. The input signals are first passed to 25 different feature maps using the selected filters. We then apply the convolutional operation and average pooling on the feature maps. After a fully connected layer with 512 hidden units, the network is connected to 10 units for the classification task. We select our filters up to the distance<14 regions($\sim$ 25 steps for ballistic duffusion), and this ensures the filters gather the correlation information within reasonable regions. For pure ballistic filters, the classification accuracy is around 99.11%, when we keep the first eight ballistic filters and use different filters with different randomness, the accuracy increases to 99.39%. Our results show that the classification accuracy can be improved using a mixture of perturbed filters within certain distance region.

### 6.3 COIN OPERATOR

The ballistic walk filters can also be generalized to different coin operators. Except using Hardmard and noisy Hardmard coin operator, we can also use a discrete Fourier operator(DFO) or Grover operator, the discrete Fourier operator is written:

$$DFO = \frac{1}{d^{1/2}} \begin{bmatrix} 1 & 1 & 1 & ... & 1 \\ 1 & \omega & \omega^2 & ... & \omega^{d-1} \\ 1 & ... & ... & ... & ... \\ 1 & \omega^{d-1} & \omega^{2(d-1)} & ... & \omega^{(d-1)(d-1)} \end{bmatrix} = \frac{1}{2} \begin{bmatrix} 1 & 1 & 1 & 1 \\ 1 & \omega & \omega^2 & \omega^3 \\ 1 & \omega^2 & \omega^4 & \omega^6 \\ 1 & \omega^3 & \omega^6 & \omega^9 \end{bmatrix} \tag{3}$$

| Filter Index / Accuracy | Ballistic($\alpha = 0$) | $\alpha = 0.1$ | $\alpha = 0.15$ | $\alpha = 0.05$ | $\alpha = 0.20$ |
|---|---|---|---|---|---|
| **99.11±0.13** | 1-25 | 0 | 0 | 0 | 0 |
| **99.14±0.17** | 1-8 | 9,10 | 24,25 | 10-23 | 0 |
| **99.32±0.09** | 1-8 | 3-10 | 4-10 | 8,9 | 0 |
| **99.35±0.07** | 1-8 | 1-8 | 1-8 | 9 | 0 |
| **99.23±0.13** | 1-8 | 2,4,6,8,10,12 | 3,6,9,12,15,18 | 2,4,6,8,10 | 0 |
| **99.32±0.06** | 1-8 | 3,6,9,12 | 3,6,9,12 | 3,6,9,12 | 3,6,9,12,15 |
| **99.39±0.09** | 1-8 | 3,6,9,12 | 3,6,9,12 | 9,12,15,18 | 12,15,18,21,24 |

Table 3: Accuracy with different randomized Hardmard operations. We use 25 filters with different steps and randomness for each case.

where $\omega = e^{2\pi i/d}$ is the $d$th root of unity and the Grover operator is:

$$G = \begin{bmatrix} a & b & b & \dots & b \\ b & a & b & \dots & b \\ \dots & \dots & \dots & \dots & \dots \\ b & b & b & \dots & a \end{bmatrix} = \frac{1}{2} \begin{bmatrix} -1 & 1 & 1 & 1 \\ 1 & -1 & 1 & 1 \\ 1 & 1 & -1 & 1 \\ 1 & 1 & 1 & -1 \end{bmatrix} \tag{4}$$

where $a = (2/d) - 1$ and $b = 2/d$. The results are shown in Table 4. Note that we usually select unitary operation in the coin space to keep the probability as a constant. However, not every unitary operator results in ballistic transportation, the Grover operator will localize near the start point as the steps grow, however, they all have a speed-up effect comparing to the classical diffusive filters.

| Structure | DFO10 | DFO32 | Grover10 | Grover32 |
|---|---|---|---|---|
| Accuracy | 97.32 | 97.58 | 97.26 | 97.39 |

Table 4: Performance using Grover and DFO filters

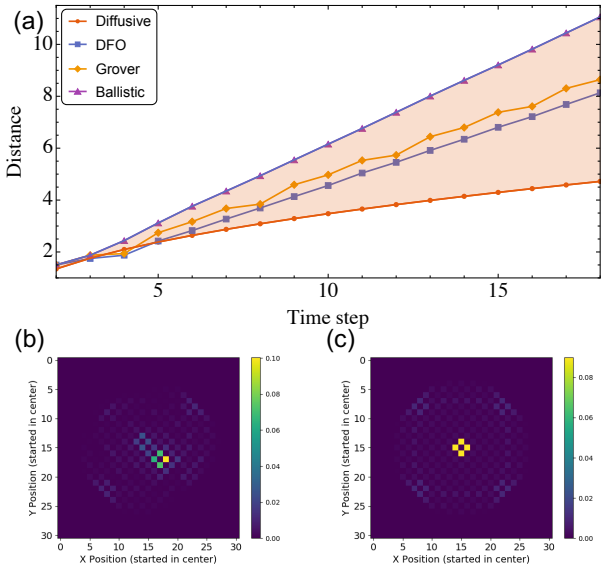


Figure 10: Comparison between DFO and Grover operator at 15 steps. (a) The transportation speed. (b) The walker's distribution after 15 steps using DFO. (c) The walker's distribution after 15 steps using Grover operator.

The DFO and Grover operator have a transportation speed between the ballistic filters and diffusive filters, thus can be seen as special forms of randomized filters. The general Hadamard coin is balanced. DFO retains the balanced properties on a general graph. Every state in coin space is obtained with

equal probability. The Grover operator helps retain the symmetry of the signal and is permutation symmetric. The Grover operator is not a balanced coin because the probability(weight in our case) does not change its propagating directions($p = (1 - 2/d)^2$).

## 7 Conclusion and Future Work

In this paper, we introduced a generalization of graph neural network: ballistic graph neural network. We started from the speed problem of the traditional diffusive kernel and tackle this problem from the perspective of transportation behaviour. We showed the linear transportation behaviour of ballistic filters and introduced the de-coherence scheme to adjust the filters' speed. Compared with diffusive filters, the ballistic filters achieve similar accuracy using 1/3 of the parameters. Besides, we showed that the efficiency of the ballistic filters could be improved by controlling transportation behaviour. Compared to the random walk method, we used two operators: the coin operator and shift operator to control the walker, and thus controlled the information the walker gathers. Our pipeline provides a new perspective for efficient extracting the graphical information using diffusion-related models.

Future work can investigate these two directions:

**The Network Structure.** In this paper, we use simplified architecture to demonstrate the concept of the ballistic walk, the layers are limited to 5 layers, and we use traditional average pooling. More layers can be added to improve particular accuracy, and more sophisticated pooling methods can be introducedDefferrard et al. (2016). Other techniques like dropout can also be employed to improve accuracy.

**The Ballistic Filter.** De-coherence can also be introduced into the shift operator. In other words, we can use perturbed shifted operator, and thus we introduce randomness in the spatial domain. We can also try different unitary operators in the coin space or change the initial state of the walker. The extension to general graphs can be generalized by adding self-loops to the nodes and thus make the graph regular.

## 8 Discussion: Ballistic Filter in one dimensional condition

The ballistic filters are inspired by two-dimensional quantum walk. The quantum coherence effect guarantees fast ballistic transportation. The different states in the coin space can be seen as the independent state from spatial behaviour, for example, the spin of fermions or the polarization of light. More information about the quantum walk can be found at Childs et al. (2003).

Why introducing ballistic filters results in better performance? We here offer a conjecture from the perspective of signal processing using one-dimensional condition.

The classical diffusion in the one-dimensional case has the shape of:

$$g(x) = \frac{a}{\pi} e^{-ax^2} \tag{5}$$

and the frequency part can be written as:

$$\hat{g}(f) = e^{\frac{\pi^2 f^2}{a}} \tag{6}$$

The $\hat{g}(f)$ decreases as $f$ increases and thus can be seen as a low pass filter. (gaussian low pass filter) For a gaussian high-pass filter, the spatial distribution is:Makandar & Halalli (2015)

$$hg(x) = C(1 - e^{\frac{-(\frac{H}{2} - x)^2}{A^2}}) \tag{7}$$

The long time probability distribution of ballistic walk is:Luo & Xue (2015)

$$P(x) = P_0 + ae^{-d\frac{(x-b)^{1.5}}{N^{0.5}}} \tag{8}$$

Figure 11 shows the distribution of gaussian high pass filter and the cumulative distribution of 24th and 25step of ballistic diffusion. These two distributions have a similar shape while the ballistic distribution has steeper edges resulted from fast transportation.

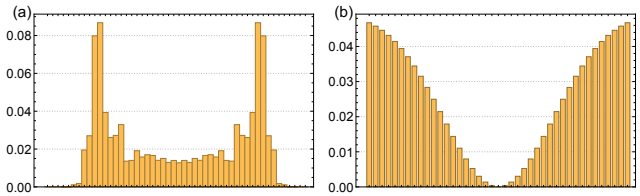


Figure 11: Different distributions. (a) cumulative distribution of 24th and 25step of ballistic diffusion. (b) Gaussian high pass filter.

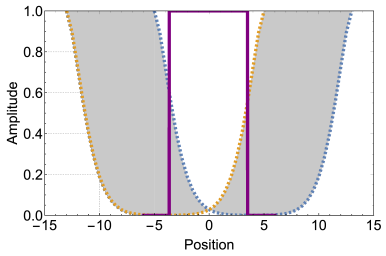


Figure 12: Ballistic diffusion with pulse signal.

The ballistic filters' capability to collect the long-time probability means it can act as a high-pass filter with different sizes. The size of the filters depends on the walking steps. Figure 12 shows the ballistic diffusion with a pulse signal from $t = -\tau$ to $t = \tau$. The orange dashed line is an approximated shape of ballistic transportation of the leftmost signal($t = -\tau$), and the blue dashed line corresponds to $t = \tau$. The width of the approximated shape is related to the walking steps. For diffusive tranporation after certain steps of difussion, the region from $t = -\tau$ to $t = -\tau$ have a gaussian shape since it is aggreated sum of gaussian distribution with centers range from $t = -\tau$ to $t = -\tau$. The classical diffusion acts like a blur filter(low pass filter). The shape of pulse signal from $t = -\tau$ to $t = \tau$ evolves to a 'valley' shape and thus the ballistic diffusion is similar to a high pass filter.

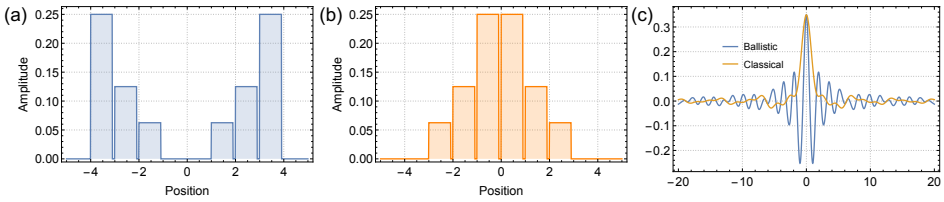


Figure 13: Schematic diagram of different filters and their Fourier transformation.

Figure 13 (a) and (b) shows approximate shape of the one dimensional ballistic and classical filtering result with a pulse signal from $t = -3$ to $t = 3$, respectively. Figure 13(c) shows the Fourier transformations. With faster transportation, the filters are capable of collecting more high frequency compared to localized diffusive filters.

**Acknowledgement** We thank Nvidia for donating NVIDIA DGX-1 used for this research

## REFERENCES

Mikhail Belkin, Partha Niyogi, and Vikas Sindhwani. Manifold regularization: A geometric framework for learning from labeled and unlabeled examples. *Journal of machine learning research*, 7 (Nov):2399–2434, 2006.

Joan Bruna, Wojciech Zaremba, Arthur Szlam, and Yann LeCun. Spectral networks and locally connected networks on graphs. *arXiv preprint arXiv:1312.6203*, 2013.

Andrew M Childs, Richard Cleve, Enrico Deotto, Edward Farhi, Sam Gutmann, and Daniel A Spielman. Exponential algorithmic speedup by a quantum walk. In *Proceedings of the thirty-fifth annual ACM symposium on Theory of computing*, pp. 59–68. ACM, 2003.

Michaël Defferrard, Xavier Bresson, and Pierre Vandergheynst. Convolutional neural networks on graphs with fast localized spectral filtering. In *Advances in neural information processing systems*, pp. 3844–3852, 2016.

David K Hammond, Pierre Vandergheynst, and Rémi Gribonval. Wavelets on graphs via spectral graph theory. *Applied and Computational Harmonic Analysis*, 30(2):129–150, 2011.

Mikael Henaff, Joan Bruna, and Yann LeCun. Deep convolutional networks on graph-structured data. *arXiv preprint arXiv:1506.05163*, 2015.

Bo Jiang, Ziyan Zhang, Doudou Lin, Jin Tang, and Bin Luo. Semi-supervised learning with graph learning-convolutional networks. In *Proceedings of the IEEE Conference on Computer Vision and Pattern Recognition*, pp. 11313–11320, 2019.

Thomas N Kipf and Max Welling. Semi-supervised classification with graph convolutional networks. *arXiv preprint arXiv:1609.02907*, 2016.

Yaguang Li, Rose Yu, Cyrus Shahabi, and Yan Liu. Diffusion convolutional recurrent neural network: Data-driven traffic forecasting. *arXiv preprint arXiv:1707.01926*, 2017.

Hao Luo and Peng Xue. Properties of long quantum walks in one and two dimensions. *Quantum Information Processing*, 14(12):4361–4394, 2015.

Aziz Makandar and Bhagirathi Halalli. Image enhancement techniques using highpass and lowpass filters. *International Journal of Computer Applications*, 109(14):12–15, 2015.

Bryan Perozzi, Rami Al-Rfou, and Steven Skiena. Deepwalk: Online learning of social representations. In *Proceedings of the 20th ACM SIGKDD international conference on Knowledge discovery and data mining*, pp. 701–710. ACM, 2014.

Dinh V Tran, Nicolò Navarin, and Alessandro Sperduti. On filter size in graph convolutional networks. In *2018 IEEE Symposium Series on Computational Intelligence (SSCI)*, pp. 1534–1541. IEEE, 2018.

Petar Veličković, Guillem Cucurull, Arantxa Casanova, Adriana Romero, Pietro Lio, and Yoshua Bengio. Graph attention networks. *arXiv preprint arXiv:1710.10903*, 2017.